International Journal of Biological Macromolecules 164 (2020) 37–44

Contents lists available at ScienceDirect

International Journal of Biological Macromolecules

journal homepage: http://www.elsevier.com/locate/ijbiomac

Effect of CuS reinforcement on the mechanical, water vapor barrier, UV-light barrier, and antibacterial properties of alginate-based composite films

Swarup Roy, Jong-Whan Rhim *

Department of Food and Nutrition, BioNanocomposite Research Institute, Kyung Hee University, 26 Kyungheedae-ro, Dongdaemun-gu, Seoul 02447, Republic of Korea

ARTICLE INFO

Article history:
Received 28 April 2020
Received in revised form 29 June 2020
Accepted 9 July 2020
Available online 15 July 2020

Keywords:
Alginate
CuS nanoparticles
Composite film
Mechanical property
WVP
Antibacterial activity

ABSTRACT

Alginate-based functional nanocomposite films were prepared by the incorporation of copper sulfide nanoparticles (CuSNP) using a solution casting method and characterized their properties. The optical, mechanical, water vapor barrier, surface wetting, and thermal stability properties of the nanocomposite films were tested. The antibacterial activity of the alginate/CuSNP composite film was evaluated against foodborne pathogenic bacteria, *E. coli* and *L. monocytogenes*. The morphological test showed that the CuSNP were evenly distributed in the alginate matrix. The addition of 0.5 wt% of CuSNP improved the UV-barrier, hydrophobicity, mechanical strength, and water vapor barrier properties of the alginate-based film; however, the thermal stability was not significantly influenced. The alginate/CuSNP nanocomposite film showed evident antibacterial activity against the Gram-negative (*E. coli*) bacteria, but only slightly slowed the growth rate of the Garm-positive (*L. monocytogenes*) bacteria. The alginate/CuSNP nanocomposite films with significantly improved physical and functional properties have a high potential for active food packaging applications.

1. Introduction

Recently, non-biodegradable and non-recyclable plastic packaging materials have raised serious environmental concerns regarding the generation of waste and hazardous pollutants upon disposal after use [1,2]. Currently, millions of tons of plastic waste are released annually, of which only less than 3% is recycled due to procedural difficulties and economic reasons [2]. The use of biodegradable and renewable natural biopolymers has been proposed to reduce the toxic effects and environmental problems caused by non-biodegradable plastic polymers [3–5]. Various biopolymers such as polysaccharides, proteins, lipids, and combinations thereof have been used for the replacement of synthetic plastics [2,6,7]. Among them, polysaccharide-based biopolymers have appropriate structural and mechanical properties and have been widely used to produce biodegradable films [4,8–10]. Alginate is interesting because it has excellent film-forming properties with biodegradability, biocompatibility, and abundant availability [11–13]. Alginate is obtained from brown seaweed and widely used as a gelling and emulsifying agent in the food industry [14,15]. Alginate is a copolymer composed of mannuronic acid and glucuronic acid units, and the properties of alginate mainly depend on their ratio [16]. Several reports on the application of alginate-based films and coatings have been reported [17–21]. Although alginate is a promising component for the production of biodegradable films, industrial use of alginate films has been limited due to their comparatively low mechanical and weak water vapor barrier properties [14]. For the improvement of the physical and functional properties of the alginate-based films, the incorporation of various functional materials has been tested [11–13,20–22]. In this context, the addition of nano-fillers can be a suitable method to improve the physical and functional properties of alginate-based films.

Recently, research on the manufacture of functional composite films reinforced with nanoparticles for food packaging applications has attracted considerable attention. Of the various inorganic nanoparticles, metal and metal oxide nanoparticles are most commonly used for the preparation of the functional nanocomposite films [23,24]. Metal sulfide nanomaterials have attracted attention in the last few years due to the novel optical and electronic properties [25]. CuS nanoparticles are also attractive because they exist in different stoichiometric with varying crystalline phases [26], have potent antimicrobial activity with reduced toxicity to the human body compared to metallic copper and copper compounds [27,28]. Sulfidation of copper nanoparticles (CuNP) produces copper sulfide nanoparticles (CuSNP), which is a p-type semiconductor with excellent optical and electrical properties [29]. Because CuS is non-toxic and biocompatible, it is used in a variety of biological and other applications such as drug delivery, laser light monitoring, thermoelectric, solar cells, ion storage, batteries, and photovoltaic, photocatalytic, chemical sensing, eye protection, photo-degradation of

* Corresponding author.
E-mail address: jwrhim@khu.ac.kr (J.-W. Rhim).

https://doi.org/10.1016/j.ijbiomac.2020.07.092
0141-8130/

pollutants, phototherapy, antimicrobials, and in vitro bio-sensing [28,30–33]. CuSNP is considered as an excellent candidate for biomedical applications because it has similar biocompatibility to gold nanoparticles (AuNP) and does not exhibit cytotoxic effects up to 100 μM concentration [34]. Another essential feature of CuSNP is its ability to absorb infrared radiation, which is fundamentally different from metal nanoparticles such as AuNP [35]. Compared to AuNP, CuSNP offers two crucial advantages. One is a low cost, and the other is near-infrared (NIR) absorption associated with translation applications. Unlike AuNPs, the NIR properties of CuS nanoparticles do not depend on particle shape, size, and surroundings. [34]. Recently, research on the use of CuSNP for the production of biopolymer-based functional nanocomposite films has attracted attention [28,36]. To the best of our knowledge, there are no reports of the production of composite films by integrating CuSNP into alginate to improve the physical and functional properties of biocomposite films for food packaging applications.

Therefore, the main objective of this work is to prepare functional nanocomposite films using alginate and CuSNP. The composite films were characterized using SEM, FTIR, and TGA analysis. The optical, UV-light barrier, surface wetting, water vapor barrier, mechanical properties, and antimicrobial activities of the nanocomposite films were also evaluated.

2. Materials and methods

2.1. Materials

Sodium alginate was purchased from Kanto Chemical Co., Inc. (Tokyo, Japan). Brain heart infusion broth (BHI), tryptic soy broth (TSB), and agar powder were purchased from Duksan Pure Chemicals Co., Ltd. (Gyeonggi-do, Korea). Copper acetate monohydrate, ammonia, thiourea, and glycerol were procured from Daejung Chemicals & Metals Co., Ltd. (Siheung, Gyeonggi-do, Korea). *Escherichia coli* O157:H7 ATCC 43895 and *Listeria monocytogenes* ATCC 15313 were obtained from the Korean Collection for Type Culture (KCTC, Seoul, Korea). The bacterial strains were cultured in TSB and BHI agar media, respectively, and stored at 4 °C before testing.

2.2. Synthesis and characterization of CuSNP

CuSNP was prepared using copper acetate along with thiourea and corn starch according to the previously reported method [28]. For this, 5 mL of 0.5% (w/v) corn starch solution was added dropwise to 40 mL copper acetate solution (100 mM) while stirring and heating. Then added slowly 1 mL of ammonia solution and 40 mL thiourea (100 mM) dropwise and heated at 70 °C for 1 h with constant stirring. The formation of a dark green precipitate indicates the synthesis of CuSNP. The precipitate was collected and washed with double distilled water until the pH was neutral, followed by washing with ethanol, and then dried in an oven overnight at 40 °C to completely dry CuSNP. CuSNP was dispersed in an aqueous solution (1 mg/mL).

The optical characteristics of CuSNP were tested by determining an absorption spectrum using a UV–vis spectrophotometer (Mecasys Optizen POP Series UV–vis, Seoul, Korea) in the range of 200–1100 nm. The morphological examination of CuSNP was performed using a field emission transmission electron microscope (FE-TEM, JEM-2100F, JEOL, Ltd., Tokyo, Japan), and the particle size was analyzed using ImageJ (ImageJ 1.46r, National Institute of Health, USA).

2.3. Preparation of alginate/CuSNP composite films

The alginate-based composite films were prepared using a solution casting method according to the previously described method with slight modification [37]. The procedure for the preparation of alginate-based nanocomposite films is shown in Scheme 1. Various concentrations of CuSNP (0.0, 0.5, 1.0, and 1.5 wt% based on alginate) were dispersed in 150 mL distilled water with vigorous stirring and sonicated for 20 min using a water bath-type sonicator (FS140 Ultra Cleaner, Fisher Scientific, Pittsburg, PA, USA), and homogenized at 5000 rpm for 10 min using a high shear mixer (T25 basic, Ika Labotechnik, Janke & Kunkel GmbH & Co., KG Staufen, Germany). Glycerol (30 wt% based on alginate) was then added to the above suspension and followed by slow addition of 3 g alginate and heated at 80 °C for 20 min with continuous stirring. The film-forming solution was cast on leveled Teflon film (Cole-Parmer Instrument Co., Chicago, IL, USA) coated glass plate (24 cm × 30 cm), and allowed to dry at room temperature (22 ± 2 °C) for 48 h. The dried film was peeled off from the glass plate and conditioned in a humidity chamber (model FX 1077, Jeio Tech Co. Ltd., Ansan, Korea) at 25 °C and 50% RH for at least 48 h before the further test. The prepared films were designated Alg, Alg/$CuS^{0.5}$, Alg/$CuS^{1.0}$, and Alg/$CuS^{1.5}$, depending on the concentration of CuSNP.

2.4. Film characterization and properties

2.4.1. Surface morphology

The surface morphology of the film samples was observed using a field emission scanning electron microscope (FE-SEM, S-4800, Hitachi Co., Ltd., Matsuda, Japan). A small portion of the film sample, sputter-coated with platinum using a vacuum sputter coater for 30 s, was mounted on the SEM specimen holder and observed the image. The upper surface of the film was tested for the analysis of surface morphology.

2.4.2. FTIR spectroscopy

Fourier transform infrared (FTIR) spectra of the films were recorded in an attenuated using a total reflectance-FTIR spectrophotometer

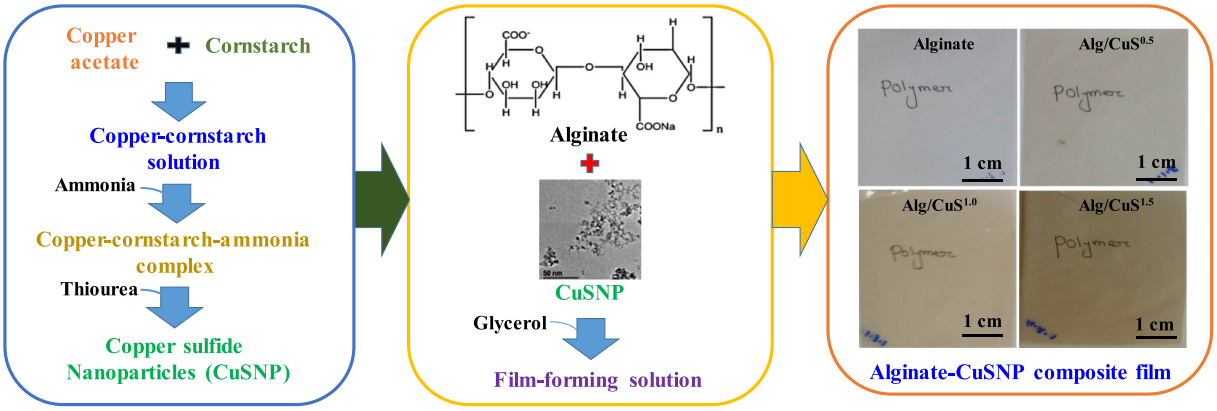

Scheme 1. A schematic representation for the development of alginate-based nanocomposite film with CuSNP.

(ATR-FTIR, TENSOR 37 Spectrophotometer with OPUS 6.0 software, Billerica, MA, USA) in the range of 4000–500 cm^{-1} with the resolution of 32 scans at 4 cm^{-1}. For this, all film samples were cut into rectangular shapes (5 cm × 5 cm) and directly placed on the ray exposing stage. Background calibration of all spectra was performed using the air spectrum.

2.4.3. Thermal stability

The thermal stability of the film samples was tested by thermogravimetric analysis (TGA) using a thermogravimetric analyzer (Hi-Res TGA 2950, TA Instrument, New Castle, DE, USA). About 10 mg of each film sample was taken in a standard aluminum cup and scanned at a heating rate of 5 °C/min in the temperature range of 30–600 °C with a nitrogen flow of 50 cm^3/min, and an empty cup was used as a reference [38]. The maximum disintegration temperature (T_{max}) at each thermal degradation step was determined from a derivative from of TGA (DTG) curve.

2.4.4. Optical properties

The apparent color of the film sample was estimated using a Chroma meter (Konica Minolta, CR-400, and Tokyo, Japan) with a standard white color plate (L = 97.75, a = −0.49, and b = 1.96) as a reference. The color of the film sample was defined as L (lightness), a (redness/greenness) and b (yellowness/blueness) values. The total color difference (ΔE) was calculated as follows:

$$\Delta E = \left[(\Delta L)^2 + (\Delta a)^2 + (\Delta b)^2\right]^{0.5} \quad (1)$$

where ΔL, Δa, and Δb is the difference between each color values of the standard color plate and film specimen, respectively.

The optical properties of the alginate-based film samples were evaluated by measuring the light absorption spectra and the transmittance of the films. Each film was cut into squares (5 cm × 5 cm) and placed between the magnetic holders of the spectrophotometer. The light absorbance and percent transmittance were measured using a UV–vis spectrophotometer (Mecasys Optizen POP Series UV/Vis, Seoul, Korea). The light absorbance of the composite film was recorded in the range of 200–1100 nm. UV-barrier property and transparency of the films were evaluated by measuring percent light transmittance at 280 nm (T_{280}) and 660 nm (T_{660}), respectively [28].

2.4.5. The thickness and mechanical properties

The film thickness was measured using a digital micrometer (Digimatic Micrometer, QuantuMike IP 65, Mitutoyo, Japan) with an accuracy of 0.001 mm. The thickness of five random points was measured, and the average value was used as the film thickness.

For mechanical properties, an Instron Universal Testing Machine (Model 5565, Instron Engineering Corporation, Canton, MA, USA) was used to determine the tensile strength (TS), elongation at break (EB), and elastic modulus (EM) following the standard ASTM method D 882-88. For this, rectangular film strips (2.54 cm × 15 cm) were cut using a precision double blade cutter (model LB.02/A, Metrotec, S.A., San Sebastian, Spain) and attached to the Instron machine. The initial grip separation of 50 mm and a crosshead speed of 50 mm/min was used for the test. The TS was determined by dividing the maximum load (N) by the initial cross-sectional area (m^2) of the film sample, the EB was determined by dividing the extension at the rupture of the film by the initial length of the film (50 mm) multiplied by 100, the EM was calculated using the slope of the initial linear portion of the stress-strain curve [39].

2.4.6. Water vapor permeability (WVP) and water contact angle (WCA)

First, the water vapor transmission rate (WVTR) of the film sample was determined at 25 °C under 50% RH conditions using water vapor transmission measuring cups according to the ASTM E96–95 standard method. For this, a test film (7.5 cm × 7.5 cm) was placed on the top of a WVP cup (2.5 cm depth and 6.8 cm diameter) containing 18 mL of distilled water and sealed to prevent leakage. Then the assembled cup was kept in a humidity chamber (model FX 1077, Jeio Tech Co. Ltd., Ansan, Korea) controlled at 25 °C and 50% RH and the weight change of the cup was measured every hour for 8 h. The WVTR (g/m^2. s) was determined from the slope of the plot of the weight change of the cup vs. time, and the WVP ($g \cdot m/m^2 \cdot Pa \cdot s$) of the film was calculated as follows:

$$WVP = (WVTR \times L)/\Delta p \quad (2)$$

where L was the mean film thickness (m), and Δp was the partial water vapor pressure difference across the two sides of the film, which was calculated following the method proposed by Gennadios et al. [40].

The surface wettability of the films was evaluated by measuring water contact angle (WCA) using a WCA analyzer (Phoneix 150, Surface Electro Optics Co., Ltd., Gunpo, Korea). For the measurement, the film sample (3 cm × 10 cm) was placed on the horizontal movable stage (Black Teflon coated steel, 7 cm × 11 cm) of the contact angle analyzer. Then 10 μL of water drop was added to the surface of the film using a syringe and then measured the contact angle [41].

2.5. Antibacterial activity

The antibacterial activity of the alginate-based films was tested against foodborne pathogenic bacteria, *L. monocytogenes* (Gram-positive bacteria) and *E. coli* (Gram-negative bacteria) using a colony count method [37]. For this, the bacterial strains were aseptically inoculated into TSB and BHI broth, respectively, and cultured overnight at 37 °C. After proper dilution of the cultured broth, 200 μL of the diluted inoculum (10^8–10^9 CFU/mL) was transferred aseptically to 50 mL of TSB and BHI broth containing 200 mg of the film samples to get approximately 10^5 and 10^6 CFU/mL of bacterial concentration and incubated at 37 °C for 12 h with mild shaking. Samples were withdrawn every 3 h interval and plated on agar plates after serial dilution to determine viable cell counts. In addition, the antibacterial activity of the culture broth without film and culture broth with the neat alginate film was tested for comparison. Antibacterial tests were done in triplicate with separately prepared films.

2.6. Statistical analysis

The film properties were measured in triplicate with separately prepared films as replicated experimental units. One-way analysis of variance (ANOVA) was performed, and the significant difference ($p < 0.05$) between treatment groups was determined by Duncan's multiple range test using the statistical analysis software (SPSS Inc., Chicago, IL, USA).

3. Results and discussion

3.1. Synthesis and characterization of CuSNP

CuSNP was synthesized using copper acetate and thiourea as a source of copper and sulfur, respectively. The formation of CuSNP was confirmed by the change in apparent color and light absorption pattern of the solution. The color of the solution became dark green by the formation of CuSNP [30]. Fig. 1a shows the light absorption profile of CuSNP solutions. The solution showed high UV light absorption, and the absorbance decreased as the wavelength increased to reach the minimum light absorption at 700 nm, and then increased as the wavelength increased and showed a broad absorbance in the IR region, which corresponded to the pure covellite phase of CuS [30].

The morphology of the synthesized CuSNP was observed using FETEM, and results are shown in Fig. 1b. The synthesized CuSNP was approximately spherical or irregular in shape and polydispersed. The size of the synthesized CuSNP was in the range of 3–10 nm, with an average size of 5.0 ± 1.7 nm, which is corresponding with the previously reported results [27,28].

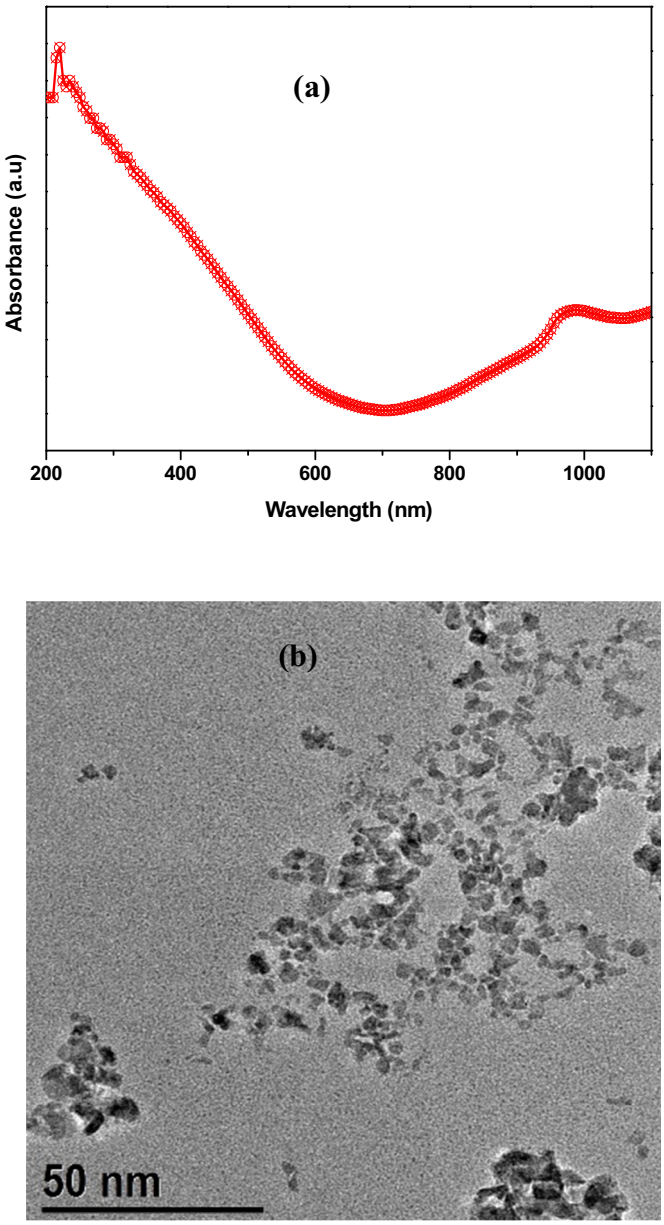

Fig. 1. UV–vis spectrum (a) and FETEM micrograph of CuSNP.

3.2. Properties of the composite film

3.2.1. Appearance and morphology

Visually, the alginate-based films were transparent and flexible with smooth-surface, as shown in Fig. 2. The neat alginate film was colorless and very transparent, but the composite film containing CuSNP showed a light greenish-brown color. The observed visual appearance of alginate-based films was similar to the agar/CuSNP composite film [28].

The FESEM images showed that the neat alginate and the composite films were intact without any apparent defects (Fig. 3). The surface of the neat alginate film was smooth without any void and cracks, whereas the composite films showed similar morphology with a more rough surface of the film. The FESEM micrographs also showed that the CuSNP were uniformly distributed in the alginate matrix. However, the surface of the composite film became a little bit rough when a higher concentration (1.5 wt% based on alginate) of CuSNP was incorporated, which was due to the agglomeration of the nanoparticles, as shown in the FESEM images. A similar phenomenon of aggregation of CuSNP was observed in the agar/CuSNP nanocomposite film when 2 wt% of CuSNP was incorporated [28].

3.2.2. FTIR

The FTIR spectra of the neat alginate and alginate-based nanocomposite films are shown in Fig. 4. All the film showed a peak at 3280 cm^{-1}, which was corresponding to the O—H stretching of alginate [42]. The peaks around 2935 cm^{-1} were due to C—H stretching vibrations of alkane groups in the biopolymer chain. The peaks appeared at 1600 cm^{-1}, and 1410 cm^{-1} were due to the symmetric and asymmetric COO^- stretching vibration of the carboxyl groups [16]. The peak at 1025 cm^{-1} was assigned to the stretching vibration of C-O-C- groups [21]. In the nanocomposite film, similar peaks with high or low intensities were observed compared to the neat alginate film. The FTIR results showed that there were no notable changes in functional groups in composite films blended with the CuSNP. These results indicated that no new chemical interaction occurred between the alginate and CuSNP; only changes in peak intensities were observed due to van der Walls interactions between CuSNP and alginate [43].

3.2.3. Thermal stability

The thermal stability of the alginate-based films was tested using TGA analysis, and the resulting TGA and DTG thermograms are shown in Fig. 5. All the alginate-based films showed two-step stages of thermal decomposition patterns. The initial stage of weight loss occurred at 80–120 °C was due to the evaporation of moisture, and the next step of thermal degradations occurred at 190–250 °C was attributed to the evaporation of glycerol as well as thermal degradation of the alginate matrix [21]. The onset temperature for the second stage of thermal decomposition of the composite films was similar to that of the neat alginate film.

The char content left after thermal degradation at 600 °C was 35.3%, 35.0, and 36.9% for the neat alginate film, the composite films incorporated with 0.5 and 1.5 wt% of CuSNP, respectively. The addition of CuSNP did not significantly influence the thermal stability of the alginate film. Similarly, there have been several studies reported that the addition of CuSNP to agar [28], the addition of halloysite nanotubes [21], or CuONP [44] to alginate films did not change the thermal stability.

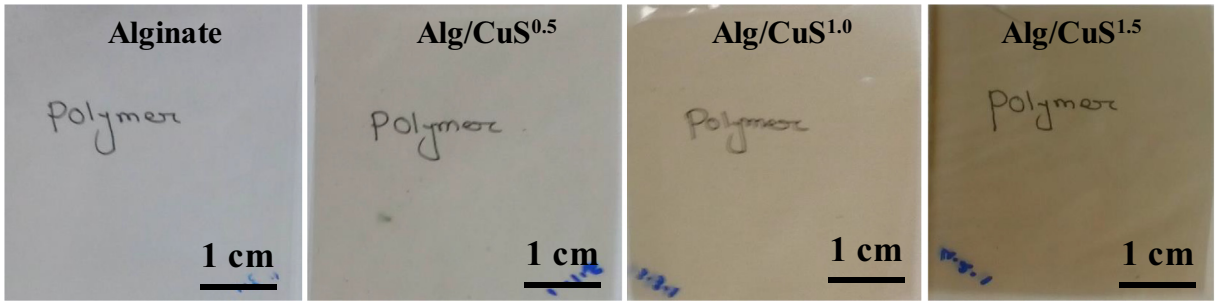

Fig. 2. The visual appearance of the alginate-based nanocomposite films.

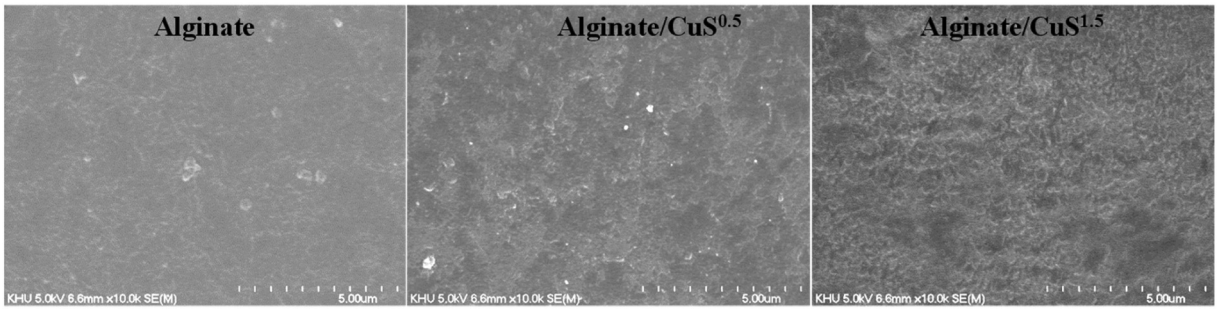

Fig. 3. FESEM micrograph of alginate/CuSNP nanocomposite films.

3.2.4. Surface color and optical properties

The neat alginate film was transparent without any color, whereas the composite films incorporated with CuSNP were greenish. Table 1 shows the surface color values of the alginate-based films evaluated using the Hunter Lab system. By the addition of CuSNP, the Hunter *L*-value (the lightness) of the film decreased significantly ($p < 0.05$), while Hunter *a*-value (greenness/redness) and Hunter *b*-value (blueness/yellowness) increased significantly ($p < 0.05$), indicating that the lightness of the film decreased, and the redness and yellowness of the film increased. As a result, the ΔE of the composite films was significantly increased compared to the neat alginate films. A similar change in surface color was observed in the agar-based composite films incorporated with CuSNP [28].

Fig. 6 shows the UV–visible light transmittance spectra of alginate-based films. The neat alginate film exhibited high light transmittance to UV and visible lights. The light transmittance of the alginate-based film decreased in all wavelength ranges by the addition of CuSNP, and the degree of reduction was dependent on the CuSNP concentration, which was mainly due to the light absorption capacity of CuSNP as evidenced by the light absorption test results (Fig. 1a). It is interesting to note that the alginate films incorporated with 1.0 wt% and 1.5 wt% of CuSNP (Alg/CuS$^{1.0}$ and Alg/CuS$^{1.5}$) showed a clear maximum light transmittance value at 700 nm, which was due to the maximum light absorption by CuSNP at 700 nm (Fig. 1a). UV-barrier property and transparency of the film was evaluated by determining the light transmittance at 280 nm (T_{280}) and 660 nm (T_{660}), respectively, and the results are also shown in Table 1.

The neat alginate film was very transparent to both UV and visible light with the T_{280} and T_{660} being 68.5 ± 1.6% and 87.6 ± 0.2%, respectively, and the transmittance decreased significantly by the addition of CuSNP. Both light transmittances decreased linearly with the concentration of CuSNP. However, the decreasing rate was more rapid in UV light (T_{280}) than visible light (T_{660}). These results indicate that the addition of CuSNP can impart UV barrier properties while less reducing the transparency of the alginate film. For example, the addition of 1.5 wt% CuSNP reduced the T_{280} of the alginate film by 82.5%, while reducing only 58.4% of the T_{660}. However, the alginate film containing 1.5 wt% CuSNP still had a see-through property. Similar light transmittance properties were observed in CuSNP-incorporated agar films [28]. CuSNP-incorporated alginate films with decreased T_{280} can be used for UV-barrier packaging film.

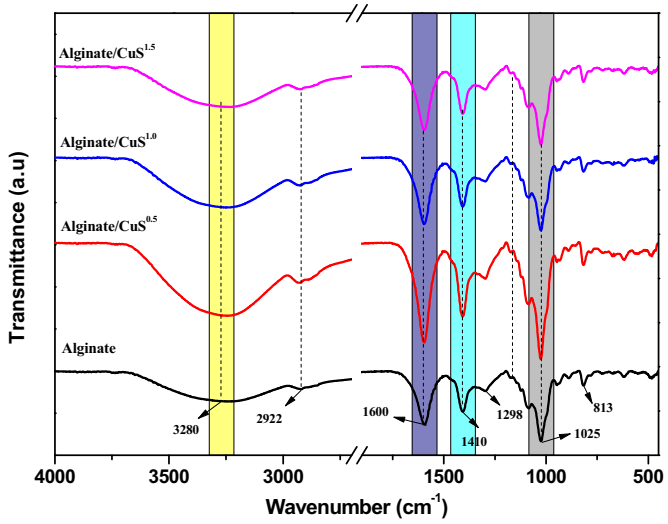

Fig. 4. FTIR spectra of alginate/CuSNP nanocomposite film.

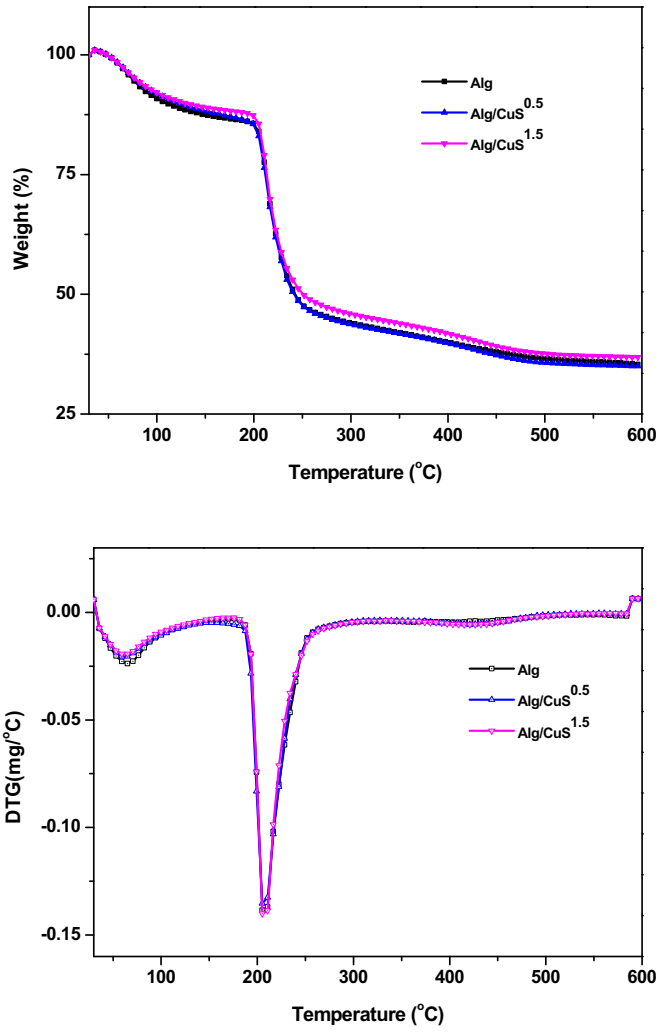

Fig. 5. TGA (a) and DTG (b) thermograms of alginate/CuSNP nanocomposite film.

Table 1
Surface color and transmittance of alginate/CuSNP nanocomposite films.

Films	L	a	b	ΔE	T_{280} (%)	T_{660} (%)
Alg	91.3 ± 0.2^{d}	−0.53 ± 0.01^{a}	5.8 ± 0.2^{a}	1.6 ± 0.2^{a}	68.5 ± 1.6^{d}	87.6 ± 0.2^{d}
Alg/CuS$^{0.5}$	83.1 ± 0.6^{c}	0.07 ± 0.11^{b}	10.3 ± 0.3^{b}	10.8 ± 0.7^{b}	44.9 ± 3.2^{c}	76.4 ± 0.4^{c}
Alg/CuS$^{1.0}$	75.8 ± 0.5^{b}	0.13 ± 0.33^{b}	15.5 ± 0.1^{c}	19.8 ± 0.4^{c}	26.3 ± 0.4^{b}	67.6 ± 0.5^{b}
Alg/CuS$^{1.5}$	68.6 ± 2.1^{a}	0.20 ± 0.20^{b}	18.7 ± 0.8^{d}	27.6 ± 2.2^{d}	12.0 ± 2.4^{a}	55.3 ± 1.4^{a}

The values are presented as mean ± standard deviation. Any two means in the same column, followed by the same letter are not significantly ($p > 0.05$) different from Duncan's multiple range tests.

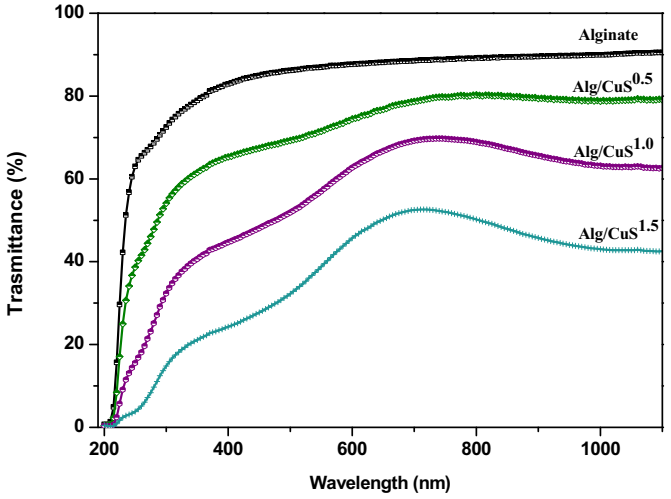

Fig. 6. UV–vis transmittance spectra of alginate/CuSNP nanocomposite film.

3.2.5. Mechanical properties

The mechanical properties of the alginate-based films are shown in Table 2. The thickness of the neat alginate film was 33.2 ± 1.3 μm, increased significantly ($p < 0.05$) by the addition of CuSNP, and increased to 41.2 ± 1.5 μm when 1.5 wt% of CuSNP was added. The increased thickness was mainly due to the increase in the dry matter by the addition of CuSNP. The mechanical properties, such as the strength, flexibility, and stiffness determined by the TS, EB, and EM, respectively, of the alginate-based films were also affected by the addition of CuSNP. The TS of the neat alginate film was 41.1 ± 0.3 MPa, which increased significantly by the addition of CuSNP up to 1.0 wt%, then decreased when added 1.5 wt% of CuSNP. However, the flexibility of the film (i.e., the EB) significantly increased by the addition of CuSNP. Similar to the strength (TS) of the film, the stiffness (EM) of the film increased when added a low amount of CuSNP (0.5 wt%) and decreased when the concentration of CuSNP increased. The increased TS of alginate film by the addition of less than 1.0 wt% CuSNP can be attributed to the increased interfacial surface interactions between the alginate and CuSNP. However, the decreased strength and stiffness of the film at higher content of CuSNP may probably be due to the aggregation of the nanoparticles, as observed in the SEM results (Fig. 3). Similar effects of nanoparticles on the mechanical properties have been observed in agar-based films incorporated with CuSNP [28] and alginate-based films incorporated with CuONP [44].

3.2.6. WVP and WCA

The water vapor barrier and surface wettability properties of the alginate-based films determined by the WVP and WCA, respectively, are also shown in Table 2. The WVP of the neat alginate film was 1.55 ± 0.06 × 10^{-9} g m/m^2.Pa.s and significantly decreased ($p < 0.05$) by the addition of CuSNP, which reduced down to 1.16 ± 0.03 × 10^{-9} g·m/m^2·Pa·s (25% reduction) when added low amount of CuSNP (0.5 wt%). Though the WVP increased slightly by the addition of CuSNP more than 0.5 wt%, the difference was not statistically significant ($p > 0.05$). A similar effect of nanofillers on the WVP was observed in the agar/CuSNP and alginate/CuONP composite films [28,44]. The reduced WVP of the composite film probably appears to be due to an increase in the path length for water vapor diffusion formed by water vapor impermeable CuSNP distributed in the alginate matrix [44].

The surface wettability of the film was evaluated by measuring the WCA of the film. WCA is generally used as a criterion for determining the hydrophilicity or hydrophobicity of a film. In general, biopolymer films with a WCA of less than 65° are considered hydrophilic surfaces [45]. The WCA of the neat alginate film was 55.7 ± 3.0°, indicating the alginate film has a hydrophilic surface. The WCA of alginate film increased significantly by the addition of CuSNP, and the increase was dependent on the CuSNP concentration. The increased WCA of the alginate/CuSNP composite films was due to the presence of hydrophobic CuSNP. Similar WCA increases were also observed in the agar/CuSNP and alginate/CuONP composite films [28,44].

3.3. Antimicrobial activity

The antimicrobial activity of the alginate-based films was tested against foodborne pathogenic bacteria, *E. coli* and *L. monocytogenes*, and results are shown in Fig. 7. As expected, the neat alginate film did not show any antibacterial activity, but CuSNP incorporated alginate films showed antibacterial activity depending on the type of bacteria as well as the concentration of CuSNP. The alginate/CuSNP composite films showed stronger antibacterial activity against Gram-negative bacteria (*E. coli*) than Gram-positive bacteria (*L. monocytogenes*). Obviously, the higher the concentration of CuSNP, the higher the antibacterial activity against both types of bacteria. In the case of *E. coli*, the composite film showed only a bactericidal effect at a low concentration of CuSNP (0.5 wt%), but it showed a strong bactericidal effect that completely destroyed the bacteria after 12 h incubation at a higher concentration of CuSNP (1.5 wt%). On the other hand, the alginate/CuSNP composite film only delayed the growth of the Gram-positive bacteria (*L. monocytogenes*). A similar effect of antibacterial activity was

Table 2
Mechanical, hydrophobicity and water vapor permeable properties of alginate/CuSNP nanocomposite films.

Films	Thickness (μm)	TS (MPa)	EB (%)	EM (GPa)	WCA (deg.)	WVP (×10^{-9} g·m/m^2·Pa·s)
Alg	33.2 ± 1.3^{a}	41.1 ± 0.3^{b}	8.5 ± 1.1^{a}	1.77 ± 0.11^{b}	55.7 ± 3.0^{a}	1.55 ± 0.06^{b}
Alg/CuS$^{0.5}$	39.6 ± 0.7^{b}	47.6 ± 1.4^{c}	13.7 ± 1.1^{b}	1.99 ± 0.46^{c}	63.0 ± 2.7^{b}	1.16 ± 0.03^{a}
Alg/CuS$^{1.0}$	40.1 ± 1.8^{b}	42.3 ± 1.8^{b}	14.1 ± 0.7^{b}	1.67 ± 0.06^{b}	63.4 ± 1.7^{b}	1.30 ± 0.09^{a}
Alg/CuS$^{1.5}$	41.2 ± 1.5^{b}	37.5 ± 1.7^{a}	14.8 ± 0.4^{b}	1.47 ± 0.01^{a}	65.1 ± 1.8^{c}	1.32 ± 0.12^{a}

The values are presented as mean ± standard deviation. Any two means in the same column, followed by the same letter are not significantly ($p > 0.05$) different from Duncan's multiple range tests.

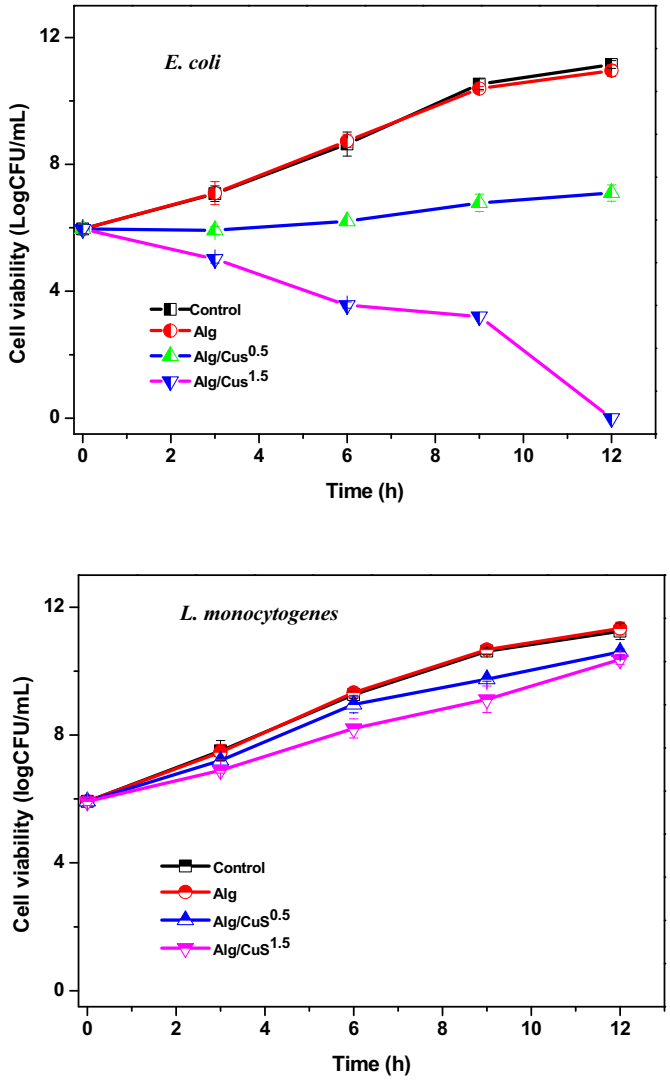

Fig. 7. Antimicrobial activity of alginate/CuSNP nanocomposite films against *E. coli* and L. *monocytogenes*.

observed in agar-based films incorporated with CuSNP and CuONP [28,38]. The different antibacterial activity of CuSNP depending on the type of bacteria is probably due to the different cell wall structures of these bacteria [46]. The thicker cell wall structure of Gram-positive bacteria (*L. monocytogenes*) probably lowers its antibacterial activity by making it more difficult to transport CuSNP into the cytoplasm. As a whole, the antimicrobial activity of CuSNP was lower than CuNP, which is due to the sulfidation of copper [47]. Sulfidation of CuNP reduces the antibacterial activity but also reduces the cytotoxicity of copper, which is advantageous for biological applications [28]. The antibacterial action of CuSNP has not been clearly elucidated yet, but it is believed that free copper ions (Cu^{++}) can interact with the negatively charged cell membrane protein and destroy the cell wall. [48]. Another plausible explanation is the interaction of CuSNP with bacteria, which activates intracellular free radical species-mediated oxidative damage to antioxidant defenses and damages cell membranes, leading to cell death [30].

4. Conclusions

CuSNP was prepared by the sulfidation of CuNP and used for the preparation of alginate-based functional composite films. The addition of CuSNP affected the physical and functional properties of the alginate-based composite films. The addition of CuSNP improved the mechanical and water vapor barrier properties of the alginate-based films. In addition, it showed UV barrier properties while maintaining the see-through properties of the composite film. The alginate/CuSNP composite films showed potent antimicrobial activity against foodborne pathogenic Gram-negative bacteria, *E. coli*, but exhibited only a slight activity to delay the growth of Gram-positive bacteria, *L. monocytogenes*. The alginate/CuSNP composite films with improved physical and functional properties can be used for active food packaging applications.

Author statement

Swarup Roy: Designed the experiments, Data acquisition, Data analysis, and Original draft preparation.

Jong-Whan Rhim: Supervision, Review, Editing, Funding and Resources.

Acknowledgment

This work was supported by the National Research Foundation of Korea (NRF) grant funded by the Korea government (MSIT) (No. 2019R1A2C2084221).

References

[1] D.S. Cha, M.S. Chinnan, Biopolymer-based antimicrobial packaging: a review, Crit. Rev. Food Sci. Nutr. 44 (2004) 223–237.
[2] C.G. Otoni, R.J. Avena-Bustillos, H.M.C. Azeredo, M.V. Lorevice, M.R. Moura, L.H.C. Mattoso, T.H. McHugh, Recent advances on edible films based on fruits and vegetables-a review, Compr. Rev. Food Sci. Food Saf. 16 (2017) 1151–1169.
[3] T. Hoffmann, D.A. Peters, B. Angioletti, S. Bertoli, L.P. Vieira, M.G.R. Reiter, C.K. De Souza, Potentials nanocomposites in food packaging, Chem. Eng. Trans. 75 (2019) 253–258.
[4] J.-W. Rhim, P.K.W. Ng, Natural biopolymer-based nanocomposite films for packaging applications, Crit. Rev. Food Sci. Nutr. 47 (2007) 411–433.
[5] M.G.A. Vieira, M.A. Da Silva, L.O. Dos Santos, M.M. Beppu, Natural-based plasticizers and biopolymer films: a review, Eur. Polym. J. 47 (2011) 254–263.
[6] S.A.A. Mohamed, M. El-Sakhawy, M.A.-M. El-Sakhawy, Polysaccharides, protein and lipid-based natural edible films in food packaging: a review, Carbohydr. Polym. 116178 (2020).
[7] V. Siracusa, P. Rocculi, S. Romani, M.D. Rosa, Biodegradable polymers for food packaging: a review, Trends Food Sci. Technol. 19 (2008) 634–643.
[8] K.M. Zia, S. Tabasum, M. Nasif, N. Sultan, N. Aslam, A. Noreen, M. Zuber, A review on synthesis, properties and applications of natural polymer based carrageenan blends and composites, Int. J. Biol. Macromol. 96 (2017) 282–301.
[9] Cabrera-Barjas Nešić, Davidović Dimitrijević-Branković, Delattre Radovanović, Prospect of polysaccharide-based materials as advanced food packaging, Molecules 25 (2019) 135.
[10] S. Roy, L. Van Hai, H.C. Kim, L. Zhai, J. Kim, Preparation and characterization of synthetic melanin-like nanoparticles reinforced chitosan nanocomposite films, Carbohydr. Polym. 231 (2020), 115729. .
[11] Z. Mahcene, A. Khelil, S. Hasni, P.K. Akman, F. Bozkurt, K. Birech, M.B. Goudjil, F. Tornuk, Development and characterization of sodium alginate based active edible films incorporated with essential oils of some medicinal plants, Int. J. Biol. Macromol. 145 (2019) 124–132.
[12] M. Cheng, J. Wang, R. Zhang, R. Kong, W. Lu, X. Wang, Characterization and application of the microencapsulated carvacrol/sodium alginate films as food packaging materials, Int. J. Biol. Macromol. 141 (2019) (2020) 259–267.
[13] A. Abbaszad Rafi, M. Mahkam, Preparation of magnetic pH-sensitive film with alginate base for colon specific drug delivery, Int. J. Polym. Mater. Polym. Biomater. 64 (2015) 214–219.
[14] M. Gomaa, M.A. Fawzy, A.F. Hifney, K.M. Abdel-Gawad, Use of the brown seaweed Sargassum latifolium in the design of alginate-fucoidan based films with natural antioxidant properties and kinetic modeling of moisture sorption and polyphenolic release, Food Hydrocoll. 82 (2018) 64–72.
[15] K.R. Aadil, D. Prajapati, H. Jha, Improvement of physcio-chemical and functional properties of alginate film by Acacia lignin, Food Packag. Shelf Life 10 (2016) 25–33.
[16] S. Kim, S.-K. Baek, K. Bin Song, Physical and antioxidant properties of alginate films prepared from *Sargassum fulvellum* with black chokeberry extract, Food Packag. Shelf Life 18 (2018) 157–163.
[17] F. Bagheri, M. Radi, S. Amiri, Drying conditions highly influence the characteristics of glycerol-plasticized alginate films, Food Hydrocoll. 90 (2019) 162–171.
[18] T.S. Parreidt, K. Müller, M. Schmid, Alginate-based edible films and coatings for food packaging applications, Foods 7 (2018) 170.
[19] M. Bruchet, A. Melman, Fabrication of patterned calcium cross-linked alginate hydrogel films and coatings through reductive cation exchange, Carbohydr. Polym. 131 (2015) 57–64.

[20] S. Shankar, L.-F. Wang, J.-W. Rhim, Preparations and characterization of alginate/silver composite films: effect of types of silver particles, Carbohydr. Polym. 146 (2016) 208–216.
[21] S. Shankar, S. Kasapis, J.-W. Rhim, Alginate-based nanocomposite films reinforced with halloysite nanotubes functionalized by alkali treatment and zinc oxide nanoparticles, Int. J. Biol. Macromol. 118 (2018) 1824–1832.
[22] A.M. Youssef, S.M. El-Sayed, Bionanocomposites materials for food packaging applications: concepts and future outlook, Carbohydr. Polym. 193 (2018) 19–27.
[23] S.H. Othman, Bio-nanocomposite materials for food packaging applications: types of biopolymer and nano-sized filler, Agric. Agric. Sci. Procedia 2 (2014) 296–303.
[24] K. Saravanakumar, A. Sathiyaseelan, A.V.A. Mariadoss, H. Xiaowen, M.H. Wang, Physical and bioactivities of biopolymeric films incorporated with cellulose, sodium alginate and copper oxide nanoparticles for food packaging application, Int. J. Biol. Macromol. 153 (2020) 207–214.
[25] P.A. Ajibade, N.L. Botha, Synthesis and structural studies of copper sulfide nanocrystals, Results Phys. 6 (2016) 581–589.
[26] P.A. Ajibade, N.L. Botha, Synthesis, optical and structural properties of copper sulfide nanocrystals from single molecule presursors, Nanomaterials 7 (2017) 32.
[27] U.S. Dharsana, M.K.N.S. Varsha, A.A.K. Behlol, A. Veerappan, R. Thiagarajan, M.K.N. Sai Varsha, A.A. Khan Behlol, A. Veerappan, R. Thiagarajan, Sulfidation modulates the toxicity of biogenic copper nanoparticles, RSC Adv. 5 (2015) 30248–30259.
[28] S. Roy, J.-W. Rhim, L. Jaiswal, Bioactive agar-based functional composite film incorporated with copper sulfide nanoparticles, Food Hydrocoll. 93 (2019) 156–166.
[29] P.L. Saldanha, R. Brescia, M. Prato, H. Li, M. Povia, L. Manna, V. Lesnyak, Generalized one-pot synthesis of copper sulfide, selenide-sulfide, and telluride-sulfide nanoparticles, Chem. Mater. 26 (2014) 1442–1449.
[30] K.B.A. Ahmed, V. Anbazhagan, Synthesis of copper sulfide nanoparticles and evaluation of in vitro antibacterial activity and in vivo therapeutic effect in bacteria-infected zebrafish, RSC Adv. 7 (2017) 36644–36652.
[31] S. Goel, F. Chen, W. Cai, Synthesis and biomedical applications of copper sulfide nanoparticles: from sensors to theranostics, Small 10 (2014) 631–645.
[32] M. Ghaedi, M. Yousefi-Nejad, M. Safarpoor, H.Z. Khafri, I. Tyagi, S. Agarwal, V.K. Gupta, Synthesis of CuS nanoparticles and evaluation of its antimicrobial properties in combination with *Linum usitatissimum* root and shoot extract, Desalin. Water Treat. 57 (2016) 24456–24466.
[33] R. Cai, J. Chen, J. Zhu, C. Xu, W. Zhang, C. Zhang, W. Shi, H. Tan, D. Yang, H.H. Hng, T.M. Lim, Q. Yan, Synthesis of CuxS/Cu nanotubes and their lithium storage properties, J. Phys. Chem. C 116 (2012) 12468–12474.
[34] Z. Xiao, CuS nanoparticles: clinically favorable materials for photothermal applications? Nanomedicine 9 (2014) 373–375.
[35] Y. Li, W. Lu, Q. Huang, C. Li, W. Chen, Copper sulfide nanoparticles for photothermal ablation of tumor cells, Nanomedicine 5 (2010) 1161–1171.
[36] X. Huang, N. Hu, X. Wang, Y.S. Zhang, R. Sun, Copper sulfide nanoparticle/cellulose composite paper: room-temperature green fabrication for NIR laser-inducible ablation of pathogenic microorganisms, ACS Sustain. Chem. Eng. 5 (2017) 2648–2655.
[37] S. Roy, S. Shankar, J.-W. Rhim, Melanin-mediated synthesis of silver nanoparticle and its use for the preparation of carrageenan-based antibacterial films, Food Hydrocoll. 88 (2019) 237–246.
[38] S. Roy, J.-W. Rhim, Melanin-mediated synthesis of copper oxide nanoparticles and preparation of functional Agar/CuO NP nanocomposite films, J. Nanomater. 2019 (2019) 1–10.
[39] S. Roy, J.W. Rhim, Preparation of carbohydrate-based functional composite films incorporated with curcumin, Food Hydrocoll. 98 (2020), 105302. .
[40] A. Gennadios, C.L. Weller, C.H. Gooding, Measurement errors in water vapor permeability of highly permeable, hydrophilic edible films, J. Food Eng. 21 (1994) 395–409.
[41] S. Roy, J.W. Rhim, Carboxymethyl cellulose-based antioxidant and antimicrobial active packaging film incorporated with curcumin and zinc oxide, Int. J. Biol. Macromol. 148 (2020) 666–676.
[42] M.A. Fawzy, M. Gomaa, A.F. Hifney, K.M. Abdel-Gawad, Optimization of alginate alkaline extraction technology from *Sargassum latifolium* and its potential antioxidant and emulsifying properties, Carbohydr. Polym. 157 (2017) 1903–1912.
[43] K. Shameli, M. Bin Ahmad, W.M.Z.W. Yunus, N.A. Ibrahim, R.A. Rahman, M. Jokar, M. Darroudi, Silver/poly(lactic acid) nanocomposites: preparation, characterization, and antibacterial activity, Int. J. Nanomedicine 5 (2010) 573–579.
[44] S. Shankar, L.-F. Wang, J.-W. Rhim, Preparation and properties of carbohydrate-based composite films incorporated with CuO nanoparticles, Carbohydr. Polym. 169 (2017) 264–271.
[45] E.A. Vogler, Structure and reactivity of water at biomaterial structure surfaces, Adv. Colloid Interf. Sci. 74 (1998) 69–117.
[46] S. Anitha, B. Brabu, D.J. Thiruvadigal, C. Gopalakrishnan, T.S. Natarajan, Optical, bactericidal and water repellent properties of electrospun nano-composite membranes of cellulose acetate and ZnO, Carbohydr. Polym. 87 (2012) 1065–1072.
[47] C. Levard, E.M. Hotze, B.P. Colman, A.L. Dale, L. Truong, X.Y. Yang, A.J. Bone, G.E. Brown, R.L. Tanguay, R.T. Di Giulio, E.S. Bernhardt, J.N. Meyer, M.R. Wiesner, G.V. Lowry, Sulfidation of silver nanoparticles: natural antidote to their toxicity, Environ. Sci. Technol. 47 (2013) 13440–13448.
[48] M. Safaei, M. Taran, Optimized synthesis, characterization, and antibacterial activity of an alginate-cupric oxide bionanocomposite, J. Appl. Polym. Sci. 135 (2018), 45682. .